Faculty of Mechanical and Mechatronics Engineering

Smart Hand

ME 598 Final Project Report

Prepared by:

Adrian Au, Abdeali Dhuliyawalla, and Luc Weimer

Submission Date: 26th April 2021

Table of Contents

1.0 Introduction & Motivation

Piezoelectric materials can extend or contract based on an external electric field. This unique property makes it an interesting choice for specific actuation systems that require high precision, backlash-free motion (Mishra et al.). This project is focused on exploring piezo actuation systems for prosthetic hands. In the US alone, 1.7 million individuals suffer from limb loss; 41,000 are upper limb amputees (Braza et al.). Transradial and transhumeral amputees lose their complete hands and are unable to perform simple activities of daily living. Living with this sort of disability affects someone's level of independence and quality of life. There is an increased burden on caregivers and a reduction of their emotional and physical health. These far-reaching consequences have warranted the development of advanced prosthetic devices that can replicate the motion of the human hand. Even with these advancements, the majority of patients use prosthetics for cosmetic purposes. Their functional use is often problematic due to their bulky nature, and they have a rejection rate of roughly 34% (Braza et al.). Conventional actuation systems using motors and gears can result in a heavy and cumbersome device to carry. This need motivated this project's scope and an important question: can piezoelectric actuation be a suitable choice for robotic prosthetic hands?

2.0 Literature Review

Myoelectric prosthetics utilize electrical signals from intact muscles to control the actuators found in the prosthetic limb. However, their size and weight limitations result in a need for performance trade-offs such as between range of motion, gripping force, and a total number of actuators. Examples of such commercially available hands are shown in Figure 1 below (Belter et al).

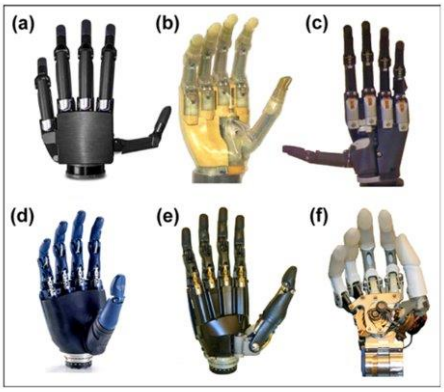

Figure 1.
(a) Vincent hand by Vincent Systems, **(b)** iLimb hand by Touch Bionics, **(c)** iLimb Pulse by Touch Bionics, **(d)** Bebionic hand by RSL Steeper, **(e)** Bebionic hand v2 by RSL Steeper, and **(f)** Michelangelo hand by Otto Bock. All hands shown without cosmetic glove.

Figure 1: Examples of existing commercial myoelectric prosthetic hands (Belter et al.)

Several considerations must be made when determining the method in which the fingers are actuated. In many hands, finger rotation is achieved through the use of motors with geared mechanical reductions. Non-backdriveable mechanisms are incorporated to allow the fingers to apply a constant gripping force without continuous stalling of the motors. When using traditional DC motors, the need for gearing and non-backdriveable mechanisms results in added weight and size. This results in it being difficult to add additional DOFs (Degrees of Freedom) without greatly complicating the system. Such systems must also be designed with built-in compliance to prevent damage in the case of overloading or impact. These systems may also be noisy to operate, and the trade-offs between speed and torque may result in movement speeds that feel" too slow" for users (Belter et al.).

Very few examples of piezoelectric actuation in human-sized robotic hands were found throughout the literature review process. However, one example that stood out was developing a single DOF thumb using a hybrid DC motor/piezoelectric stack actuator system (Levinson). Designed by an undergraduate MIT student, this project aimed to achieve a 90-degree range of motion with a max pinching force of 10 N. Levinson implemented a "tendon" style design with a DC motor used to accomplish the majority of action (0 – 90 deg) while the PZT actuator was used to achieve fine motion control (0 - 10 deg). Images of this project are shown in Figure 2 below.

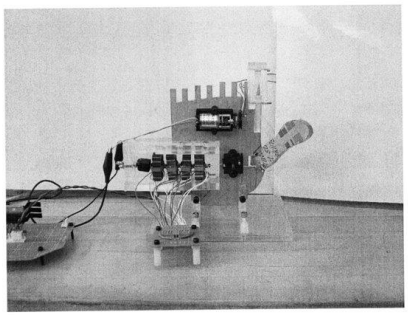

Figure 11. Front view of fully assembled hybrid DC motor/PZT actuator prototype.

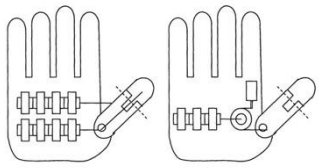

Figure 10. Potential design implementations: PZT actuator driven (left), hybrid DC motor/PZT actuator(right).

Figure 2: Example of piezoelectric actuation for the robotic thumb (Levinson)

However, several shortcomings were identified in the proposed design, including a limited range of motion from piezo stack actuators, resulting in only 10 degrees of finger rotation and limited force output. Due to the need for mechanical amplification of the piezo actuator displacement, the selected actuators only had a max force output of 5 N. Force losses associated with the routing of the tendon in addition to the location of the attachment point of the tendon to thumb resulted in the max gripping force of only 0.35 N.

3.0 Project Scope & Goals

Based on the literature review on existing solutions, functional requirements of a prosthetic hand can be developed. The project will aim to design an actuation system for a single degree of freedom finger. Design requirements for the finger are shown in Table 1 below:

Table 1: Design requirements for piezo actuated finger.

Range of motion (deg)	0° (closed) - 90° (open)
Actuation Speed (deg/s)	100
Output Force (N)	10

The range of motion and output force requirements are based on those used by Levinson's piezoelectric thumb and serve as a comparison between our design and his. Additionally, an actuation speed of 100 deg/s is selected based on the minimum finger closing speeds suggested for prosthetic hands by Belter et al.

After exploring different piezo actuation mechanisms, an inchworm actuator was chosen. A critical advantage of the inchworm system is that it is not limited in its range of motion. Piezoelectric stack actuators have minimal displacement, making it incredibly difficult to accommodate a 90-degree finger range of motion. This project aims to use the analyses covered through the course and design an 'ideal' inchworm actuator, and the proposed system architecture is shown in Figure 3 below.

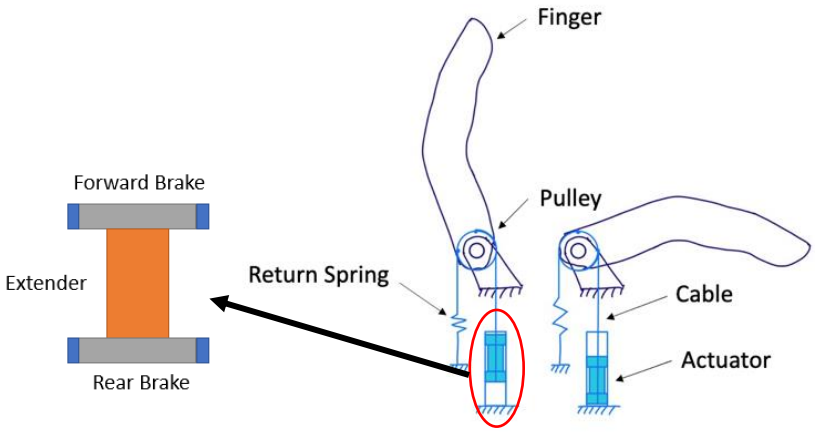

Figure 3: System architecture of 1-DOF finger and inchworm actuator.

The inchworm consists of two brake actuators and a center extender. The inchworm is directly connected to the finger through a small pulley, and a return spring brings the finger into its default open position. A series of Excel calculators were developed to help iterate through different extender and brake actuator configurations. The transient analysis was performed using custom-created MATLAB scripts. A summary of the analysis approach is shown in Figure 4.

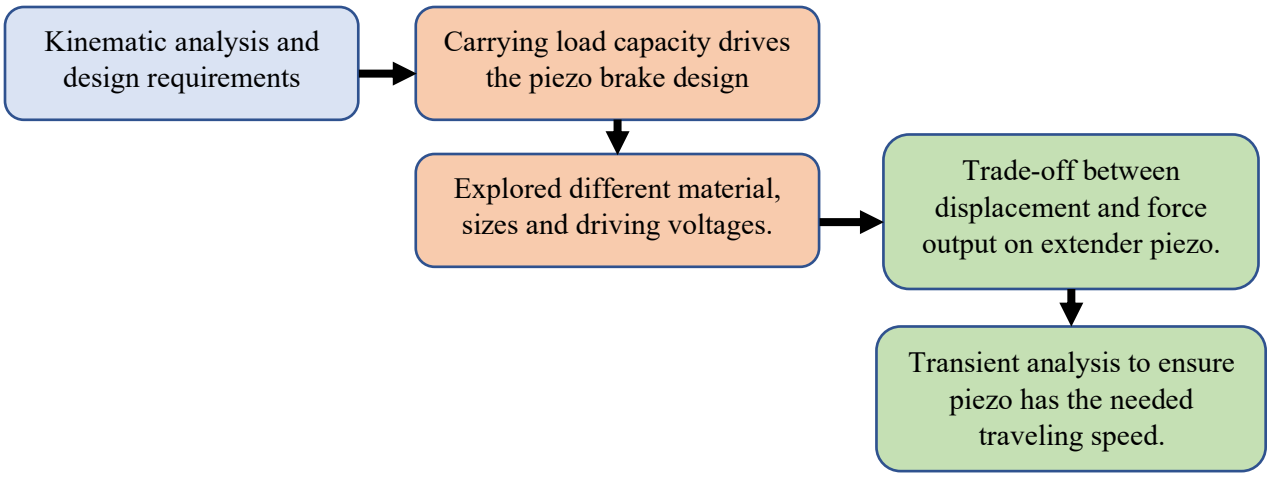

Figure 4: Summary of analysis approach.

4.0 Design Solution

4.1 Finger Kinematics

The first step in working towards an inchworm actuator is to determine the design requirements it must meet. Requirements were generated using the literature review in the previous section and assuming that the inchworm actuator will be driving a 1-DOF finger. Certain properties of the finger were considered to generate the loading cases. The finger is assumed to be 80 mm long, roughly the size of a human index finger, and it will be operating with a 90-degree range of motion. The maximum loading scenario would be a 10 N load acting on the fingertip. A coil spring with a spring constant of 0.76 N/mm is selected to bring the finger back into its default open state. A pre-tension of 1 N is applied as well. The diagram of the finger, along with the sum of moment equations, allows for the force on the actuator to be determined. This is shown in Figure 5 below.

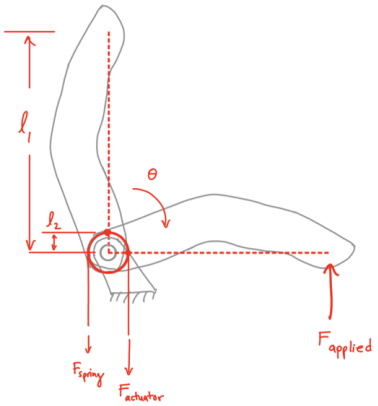

$$\sum M = F_{applied} \times l_1 + F_{spring} \times l_2 - F_{actuator} \times l_2$$
$$\Leftrightarrow F_{actuator} = F_{applied} \times \frac{l_1}{l_2} + F_{spring}$$

Also,

$$F_{spring} = \Delta l_{spring} \times k_{spring} + F_{spring,\,pretension}$$
$$\Delta l_{spring} = -\Delta l_{actuator} = l_2 \times \pi \times \frac{\theta\,[deg]}{180}$$

If $l_1 =^{**} 80\ mm,\ l_2 = 5\ mm,\ \theta = 90\ deg,\ F_{applied} = 10\ N,\ k_{spring} = 0.76\frac{N}{mm},\ F_{spring,\,pretension} = 1\ N$:

**based on approximate length of pointer finger

Figure 5: Free-body diagram of the proposed finger and sum of moments equation.

Based on the requirements for the finger, the following functional requirements for the inchworm actuator can be derived:

$$\Rightarrow \boldsymbol{F_{actuator} = 167\ N}$$

$$\Rightarrow \boldsymbol{\Delta l_{actuator} = 7.85\ mm}$$

Also, for $\dot{\theta} = 100\,\frac{deg}{s}$ (ideal actuation speed according to Belter et al.):

$$\Rightarrow \boldsymbol{actuation\ speed = 8.73\ mm/s}$$

For the robotic finger to achieve a clamping force of 10 N and close to 100 degrees per second, the inchworm actuator will need to travel at 8.7 mm/s and carry a maximum load of 167 N.

4.2 Inchworm Background

A typical inchworm actuator consists of 3 individual stack actuators, the upper and lower brakes (Brake A and Brake B), and the center extender. The inchworm is an example of a frequency-leveraged actuator, which allows for much larger displacements over time while still maintaining the high output force of the piezoelectric stack. Movement is achieved by cycling through 6 distinct steps, as shown in Figure 6 below.

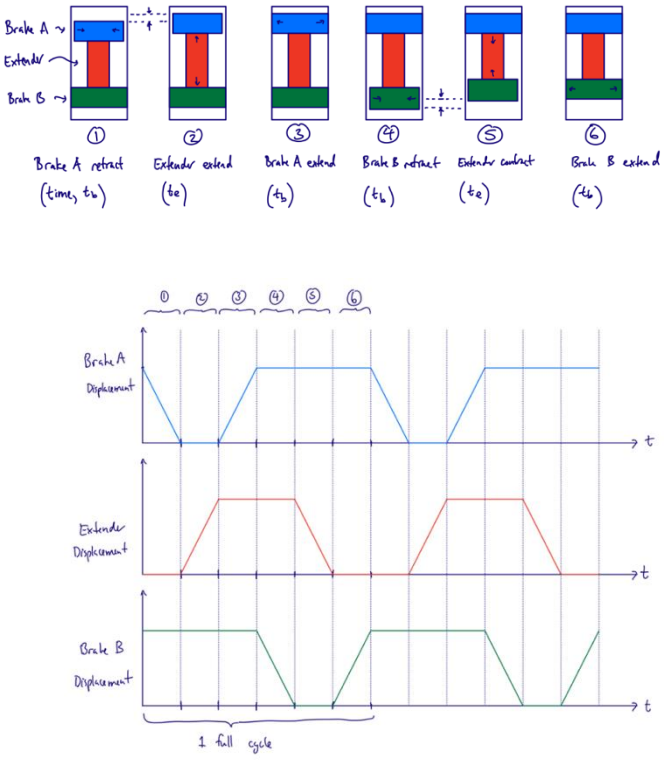

Figure 6: The six steps required for an inchworm actuator to complete a single actuation cycle

The time for one complete actuation cycle can be further broken down into the time required for the extender piezo to extend and contract ($2t_e$) and the time required for each of the brake piezo to contract and extend ($4t_b$). The actuator's cycle period can be defined as:

$$T = 2t_e + 4t_b$$

Thus, the average actuation speed can be defined as:

$$V_{avg} = \frac{\Delta l_{extender,\ per\ cycle}}{T}$$

4.3 Brake Design and Selection

Brakes for the inchworm actuator can be designed based on the carrying load requirement of 167 N. Assuming the inchworm will travel along a steel guideway, a coefficient of friction of 0.8 is selected ("Friction and Friction Coefficients"). Each piezo brake actuator will need to generate roughly 209 N of clamping force. Their geometries were designed using the equations for blocked stress and free strain and selecting an operating point of maximum work on the stress-strain diagram. This can be seen in Figure 7 below.

$$\delta_o = \frac{d_{33}L_s}{t} \times V$$

$$f_{bl} = \frac{d_{33}A}{S_{33}^E t} \times V$$

At maximum work:

$$F_3 = \left(-\frac{f_{bl}}{\delta_o}\right)\left(\frac{\delta_o}{2}\right) + f_{bl} = \frac{f_{bl}}{2}$$

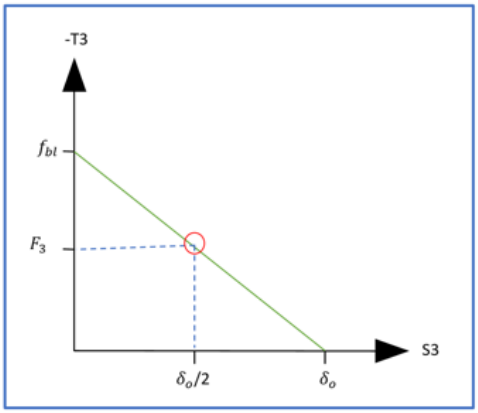

Figure 7: Brake geometry selection equations.

By substituting blocked force and free displacement into the maximum work equation, the following inequalities can be generated:

$$F_{brake} \leq F_3 = \frac{d_{33}A}{2 \times S_{33}^E t} \times V \rightarrow 3\ variable\ table$$

$$BORE_c \leq \frac{\delta_0}{2} = \frac{d_{33}L_s V}{2 \times t} = \frac{d_{33}nV}{2} \rightarrow 2\ variable\ table$$

The brake actuator must generate a force equal to or less than the specified amount F_3 which equals 209 N. Generating a braking force greater than the requirement may induce too much stress into the housing of the prosthetic hand. Excel tables were created to help select the ideal geometry, which varied the cross-sectional area, thickness, and voltage. A table was created for each type of piezo material. Similarly, the brake actuator also had a displacement requirement of 3 μm. The bore clearance was set to 3 μm, and Excel tables were created that varied the voltage and number of brake elements until the displacement was greater than or equal to 3 μm. Example tables are shown in Figure 8. These two tables show a partial view of the varied parameters; these tables correspond to the material PZT-5H with a cross-sectional geometry of 2.75x2.75mm. Each row entry corresponds to increasing layer thickness, and the columns correspond to increasing voltage. The top table shows the output force, and the bottom shows the displacement. All entries in Figure 8 are currently red which means the geometries do not meet our criteria of force and displacement. As voltage is increased, this begins to change, and the first geometry to pass is selected for each material. It is generally desirable to operate at a lower voltage, so the material that can meet the requirements with the lowest operating voltage is selected as the final option.

	PZT-5H		For A (m2):	7.53E-06	(2.75mm sides)				FORCE TABLE (N):						
							Volts (V):								
		150	152	154	156	158	160	162	164	166	168	170	172	174	
	1.00E-04	1.75E+02	1.77E+02	1.79E+02	1.82E+02	1.84E+02	1.86E+02	1.89E+02	1.91E+02	1.93E+02	1.96E+02	1.98E+02	2.00E+02	2.03E+02	
	2.00E-04	8.74E+01	8.85E+01	8.97E+01	9.09E+01	9.20E+01	9.32E+01	9.44E+01	9.55E+01	9.67E+01	9.78E+01	9.90E+01	1.00E+02	1.01E+02	
t (m):	3.00E-04	5.82E+01	5.90E+01	5.98E+01	6.06E+01	6.13E+01	6.21E+01	6.29E+01	6.37E+01	6.45E+01	6.52E+01	6.60E+01	6.68E+01	6.76E+01	
	4.00E-04	4.37E+01	4.43E+01	4.48E+01	4.54E+01	4.60E+01	4.66E+01	4.72E+01	4.78E+01	4.83E+01	4.89E+01	4.95E+01	5.01E+01	5.07E+01	
	5.00E-04	3.49E+01	3.54E+01	3.59E+01	3.63E+01	3.68E+01	3.73E+01	3.77E+01	3.82E+01	3.87E+01	3.91E+01	3.96E+01	4.01E+01	4.05E+01	
	6.00E-04	2.91E+01	2.95E+01	2.99E+01	3.03E+01	3.07E+01	3.11E+01	3.15E+01	3.18E+01	3.22E+01	3.26E+01	3.30E+01	3.34E+01	3.38E+01	
	7.00E-04	2.50E+01	2.53E+01	2.56E+01	2.60E+01	2.63E+01	2.66E+01	2.70E+01	2.73E+01	2.76E+01	2.80E+01	2.83E+01	2.86E+01	2.90E+01	
	8.00E-04	2.18E+01	2.21E+01	2.24E+01	2.27E+01	2.30E+01	2.33E+01	2.36E+01	2.39E+01	2.42E+01	2.45E+01	2.48E+01	2.50E+01	2.53E+01	
	9.00E-04	1.94E+01	1.97E+01	1.99E+01	2.02E+01	2.04E+01	2.07E+01	2.10E+01	2.12E+01	2.15E+01	2.17E+01	2.20E+01	2.23E+01	2.25E+01	
	1.00E-03	1.75E+01	1.77E+01	1.79E+01	1.82E+01	1.84E+01	1.86E+01	1.89E+01	1.91E+01	1.93E+01	1.96E+01	1.98E+01	2.00E+01	2.03E+01	

		For n (L_s/t):	50						d_o/2 TABLE (m):						
							Volts (V):								
L_s (m):	t (m):	150	152	154	156	158	160	162	164	166	168	170	172	174	
5.00E-03	1.00E-04	2.44E-06	2.47E-06	2.50E-06	2.54E-06	2.57E-06	2.60E-06	2.63E-06	2.67E-06	2.70E-06	2.73E-06	2.76E-06	2.80E-06	2.83E-06	
1.00E-02	2.00E-04	2.44E-06	2.47E-06	2.50E-06	2.54E-06	2.57E-06	2.60E-06	2.63E-06	2.67E-06	2.70E-06	2.73E-06	2.76E-06	2.80E-06	2.83E-06	
1.50E-02	3.00E-04	2.44E-06	2.47E-06	2.50E-06	2.54E-06	2.57E-06	2.60E-06	2.63E-06	2.67E-06	2.70E-06	2.73E-06	2.76E-06	2.80E-06	2.83E-06	
2.00E-02	4.00E-04	2.44E-06	2.47E-06	2.50E-06	2.54E-06	2.57E-06	2.60E-06	2.63E-06	2.67E-06	2.70E-06	2.73E-06	2.76E-06	2.80E-06	2.83E-06	
2.50E-02	5.00E-04	2.44E-06	2.47E-06	2.50E-06	2.54E-06	2.57E-06	2.60E-06	2.63E-06	2.67E-06	2.70E-06	2.73E-06	2.76E-06	2.80E-06	2.83E-06	
3.00E-02	6.00E-04	2.44E-06	2.47E-06	2.50E-06	2.54E-06	2.57E-06	2.60E-06	2.63E-06	2.67E-06	2.70E-06	2.73E-06	2.76E-06	2.80E-06	2.83E-06	
3.50E-02	7.00E-04	2.44E-06	2.47E-06	2.50E-06	2.54E-06	2.57E-06	2.60E-06	2.63E-06	2.67E-06	2.70E-06	2.73E-06	2.76E-06	2.80E-06	2.83E-06	

Figure 8: Example Excel calculators for PZT-5H with 2.75 mm side lengths.

After exploring different geometries for materials PZT-5H, PZT-5A, PZT-5J, and APC 856, the following brake actuator was selected:

Brake Selection:

- APC 856 (material selected)
- V = 194 V (operating voltage)
- $side\ length\ (\sqrt{A}) = 2.75\ mm$
- $t = 0.1\ mm$
- $n = 50$
- $L_s = 5\ mm$
- $F_3 = \frac{f_{bl}}{2} = 266\ N$
- $\frac{\delta_0}{2} = 3.01\ \mu m$
  - Therefore we can use a bore with 3 μm clearance

4.4 Extender Design & Selection

The same maximum work approach was selected to design the extender in the inchworm actuator. The maximum work equation was rearranged to isolate for the cross-sectional area and step size in the following manner:

$$side\ length = \sqrt{A} = \sqrt{\frac{2 \times F_{cable} S_{33}^E t}{d_{33} V}} \rightarrow 2\ variable\ table$$

$$step\ size = \frac{\delta_o}{2} = \frac{d_{33} L_s V}{2 \times t} = \frac{d_{33} n V}{2} \rightarrow 2\ variable\ table$$

Each equation shown above was used to generate an Excel table with the variables in red representing parameters to iterate over. This is shown in Figure 9 below. The first table represents the width (assuming square profile) needed to reach the carrying load goal of F_{cable}. The cells are formatted so that the smallest profile appears in green. The rows show an increase in layer thickness, and columns show an increase in voltage. The second table shows the extension possible under full carrying load given a size length that increases in rows. This value should be maximized.

	PZT-5H											
							Volts (V):					
	t (m):	150	152	154	156	158	160	162	164	166	168	170
	1.00E-04	2.68E-03	2.66E-03	2.65E-03	2.63E-03	2.61E-03	2.60E-03	2.58E-03	2.56E-03	2.55E-03	2.53E-03	2.52E-03
	1.10E-04	2.81E-03	2.79E-03	2.78E-03	2.76E-03	2.74E-03	2.72E-03	2.71E-03	2.69E-03	2.67E-03	2.66E-03	2.64E-03
	1.20E-04	2.94E-03	2.92E-03	2.90E-03	2.88E-03	2.86E-03	2.84E-03	2.83E-03	2.81E-03	2.79E-03	2.78E-03	2.76E-03
	1.30E-04	3.06E-03	3.04E-03	3.02E-03	3.00E-03	2.98E-03	2.96E-03	2.94E-03	2.92E-03	2.91E-03	2.89E-03	2.87E-03
	1.40E-04	3.17E-03	3.15E-03	3.13E-03	3.11E-03	3.09E-03	3.07E-03	3.05E-03	3.03E-03	3.02E-03	3.00E-03	2.98E-03
	1.50E-04	3.28E-03	3.26E-03	3.24E-03	3.22E-03	3.20E-03	3.18E-03	3.16E-03	3.14E-03	3.12E-03	3.10E-03	3.09E-03
	1.60E-04	3.39E-03	3.37E-03	3.35E-03	3.33E-03	3.31E-03	3.28E-03	3.26E-03	3.24E-03	3.22E-03	3.21E-03	3.19E-03
	1.70E-04	3.50E-03	3.47E-03	3.45E-03	3.43E-03	3.41E-03	3.39E-03	3.36E-03	3.34E-03	3.32E-03	3.30E-03	3.28E-03
	1.80E-04	3.60E-03	3.57E-03	3.55E-03	3.53E-03	3.51E-03	3.48E-03	3.46E-03	3.44E-03	3.42E-03	3.40E-03	3.38E-03
	1.90E-04	3.70E-03	3.67E-03	3.65E-03	3.62E-03	3.60E-03	3.58E-03	3.56E-03	3.54E-03	3.51E-03	3.49E-03	3.47E-03
	2.00E-04	3.79E-03	3.77E-03	3.74E-03	3.72E-03	3.70E-03	3.67E-03	3.65E-03	3.63E-03	3.61E-03	3.58E-03	3.56E-03
	2.10E-04	3.89E-03	3.86E-03	3.84E-03	3.81E-03	3.79E-03	3.76E-03	3.74E-03	3.72E-03	3.69E-03	3.67E-03	3.65E-03
	2.20E-04	3.98E-03	3.95E-03	3.93E-03	3.90E-03	3.88E-03	3.85E-03	3.83E-03	3.80E-03	3.78E-03	3.76E-03	3.74E-03
	2.30E-04	4.07E-03	4.04E-03	4.01E-03	3.99E-03	3.96E-03	3.94E-03	3.91E-03	3.89E-03	3.87E-03	3.84E-03	3.82E-03
	2.40E-04	4.15E-03	4.13E-03	4.10E-03	4.07E-03	4.05E-03	4.02E-03	4.00E-03	3.97E-03	3.95E-03	3.93E-03	3.90E-03
	2.50E-04	4.24E-03	4.21E-03	4.18E-03	4.16E-03	4.13E-03	4.11E-03	4.08E-03	4.06E-03	4.03E-03	4.01E-03	3.98E-03

SIDE LENGTH [sqrt(A)] TABLE (m):

	can be changed ->	For n (L_s/t):	231									
							Volts (V):					
L_s (m):	t (m):	150	152	154	156	158	160	162	164	166	168	170
2.31E-02	1.00E-04	1.13E-05	1.14E-05	1.16E-05	1.17E-05	1.19E-05	1.20E-05	1.22E-05	1.23E-05	1.25E-05	1.26E-05	1.28E-05
2.54E-02	1.10E-04	1.13E-05	1.14E-05	1.16E-05	1.17E-05	1.19E-05	1.20E-05	1.22E-05	1.23E-05	1.25E-05	1.26E-05	1.28E-05
2.77E-02	1.20E-04	1.13E-05	1.14E-05	1.16E-05	1.17E-05	1.19E-05	1.20E-05	1.22E-05	1.23E-05	1.25E-05	1.26E-05	1.28E-05
3.00E-02	1.30E-04	1.13E-05	1.14E-05	1.16E-05	1.17E-05	1.19E-05	1.20E-05	1.22E-05	1.23E-05	1.25E-05	1.26E-05	1.28E-05

[d_0/2] (step distance) TABLE (m):

Figure 9: Example calculators to design the piezo extender of the inchworm.

Generating the tables shown above for each material, the following geometry was chosen:

Extender Selection:

- PZT-5H (material selected)
- V = 194 V (operating voltage)
- $side\ length\ (\sqrt{A}) = 2.36\ mm$
- $t = 0.1\ mm$
- $n = 231$
- $L_s = 23.1\ mm$
- $step\ size\ [at\ max.load] = \frac{\delta_0}{2} = 14.56\ \mu m$

The transient analysis of the inchworm can be looked at, having defined the geometry of the extender and brakes.

5.0 Transient Analysis

5.1 Step size vs. Applied Force

The first step in modeling the extension speed of the inchworm actuator is to characterize how the step size of the extender will change with varying loads. Equations were developed following the analyses conducted by Edinger et al. and Ling et al. and are shown in Figure 10.

$$S = s^E T + d_{33} E = s^E \frac{-F}{A} + d_{33} \frac{V_{in}}{t_p}$$

$$\frac{\Delta x}{n t_p} = s^E \frac{-F}{A} + d_{33} \frac{V_{in}}{t_p}$$

$$F = \frac{n d_{33} A}{n t_p s^E} V_{in} - \frac{\Delta x A}{n t_p s^E} = n d_{33} K_a V_{in} - \Delta x K_a$$

$$\boldsymbol{\Delta x = n d_{33} V_{in} - \frac{F}{K_a}}$$

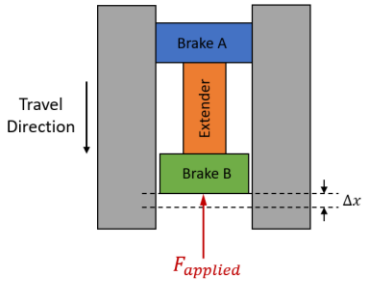

Figure 10: Equation development for extension versus applied force.

The fundamental strain equation for a piezo element can be rewritten by replacing stress with force divided by area. This force term will be negative as it opposed the direction of travel. Strain can also be further reduced as a change in the extender's height divided by the initial measurement. After the rearrangement of the equation, a common stiffness term emerges, shown by $K_a = \frac{A}{n t_p s^E}$. The final rearrangement allows for a step height, shown by Δx, to be written as a function of the piezo stack's material property, thickness, number of elements, applied voltage, and the exerted force. A design sweep can be conducted using the developed equation to analyze how different materials perform under varying loads. Geometry will be held constant, and the only difference will be the material of the piezo actuator. The geometry and other properties used in the modeling for each configuration are shown in Table 1 below. Results are shown in Figure 11 below.

Table 2:Propeties of the piezo actuator for step size modeling.

Operating Voltage	Side Length (mm)	Thickness (mm)	Number of layers
194	2.36	0.1	231

Based on Figure 11, only APC 856 and PZT-5H are competitive. APC 856 leads to higher step sizes at larger loads, and the opposite is true for PZT-5H. Since the actuator will not be performing under maximum load over its entire stroke, choosing a material that offers a larger step size will lead to faster actuation. This result also helps verify that PZT-5H is the correct material for the extending piezo stack.

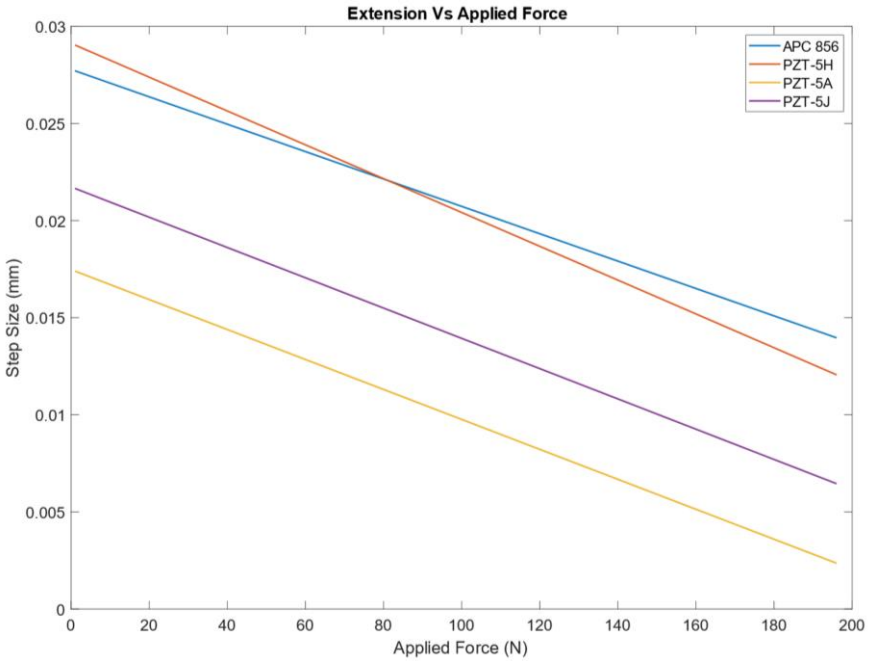

Figure 11: Step size vs. applied force for different piezo materials.

After defining the size of each step change, the next step in the transient analysis is to determine how long these extensions and contractions will take. This is looked at in the next section.

5.2 Time Response

The time taken for a piezo to reach its nominal displacement when unloaded can be approximated as (PI Ceramic, n.d.):

$$t_{min} \approx \frac{1}{3f_0}$$

Where f_0 is the resonant frequency of the actuator without load [Hz].

This response of the actuator when loaded can be approximated by replacing the resonant frequency with the effective resonant frequency as defined below (PI Ceramic, n.d.):

$$t_{min} \approx \frac{1}{3f_o}$$

Resonant Frequency (without load) [Hz]

$$f_o' = f_o \sqrt{\frac{\frac{m}{3}}{\frac{m}{3} + M}}$$

m = mass of actuator
M = mass of additional load

Worst Case Analysis: How will resonant frequency change with a 10 kg mass sitting on the stack? Actuator mass is roughly 20 grams.

$$f_o' = f_o \sqrt{\frac{\frac{20 \times 10^{-3}}{3}}{\frac{20 \times 10^{-3}}{3} + 10}} = 0.0258 f_o$$

Using the properties of commercially available stack actuators (Figure 12 and Table 3) similar in size to the actuators specified in the proposed inchworm actuator, the inchworm actuator cycle period and speed can be estimated:

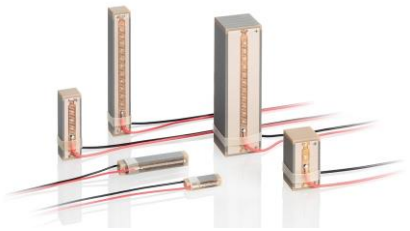

Figure 12: P-882 – P-888 PICMA® Stack Multilayer Piezo Actuators (PI USA, n.d.)

Table 3: Properties of commercially available stack actuators (PI USA, n.d.)

Actuator	Dimensions [mm]	Nominal Displacement [um]	Blocked Force [N]	Resonant Frequency, f_0 [Hz]	Loaded Frequency (10 kg mass) $0.0258 f_0$ [Hz]
Equivalent piezo for brakes: P-883.11	3 x 3 x 9	6.5	290	135,000	3,484
Equivalent piezo for extender: P-885.91	5 x 5 x 36	32	950	40,000	1,032

From the listed properties of these actuators, the theoretical maximum achievable actuation speed (when considering a worst-case load of 10 kg on all actuators) is calculated as:

$$t_{e,loaded} \approx 323.00\ \mu s$$

$$t_{b,loaded} \approx 95.68\ \mu s$$

$$T_{loaded} = 2t_{e,loaded} + 4t_{b,loaded} = 1.03\ ms$$

$$T_{loaded}^{-1} = 972\ Hz$$

$$V_{avg} = \frac{\Delta l_{extender,\ per\ cycle}}{T} = \frac{32 \times 10^{-3}\ mm}{1.03 \times 10^{-3}\ s} = 31.07\ mm/s$$

Even under a worst-case loading scenario, the actuation speed of the inchworm actuator is still faster than the required 8.73 mm/s. Thus, it can be seen that the driving frequency of the actuator (as opposed to the response time of the piezo) will be the limiting factor.

Driving this illustrative actuator at a lower frequency of 300 Hz results in achieving the target speed of 8.73 mm/s while remaining below the resonant frequency of the material.

$$V_{avg} = \Delta l_{extender,per\ cycle} \times f_{actuator} = 29.1 \times 10^{-3}\ mm \times 300\ Hz = 8.73\ mm/s$$

5.3 Time Response Simulation

Having defined the extension length versus load-carrying capacity of the extender in the inchworm actuator along with its time response, a script can be created that discreetly solves for the movement of the entire actuator against time. The script also allows the return spring force to dynamically change as the inchworm moves along its path and recalculates a new step size. The program sequentially runs through the extension and contraction of the center actuator along with the front and rear brakes and provides a distance versus time plot. The program can be broken up into four modules, as seen from Figure 13 below.

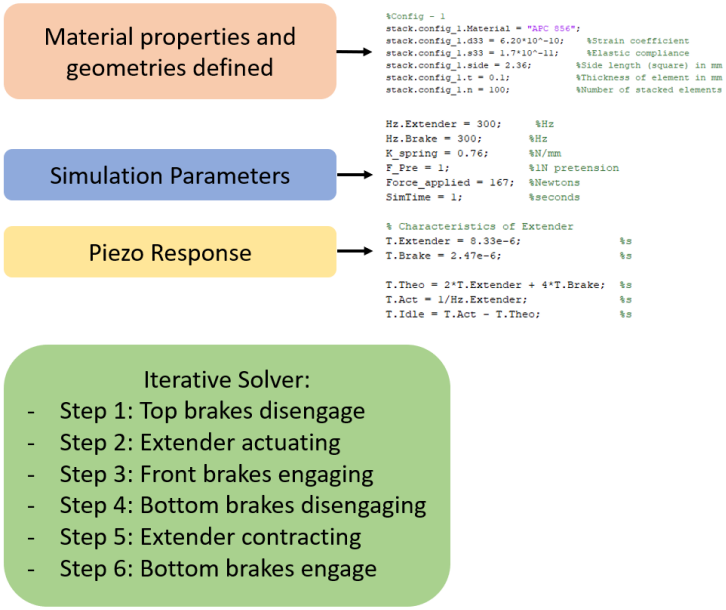

Figure 13: Summary of transient simulation script.

The 'Material properties' input allows multiple configurations of a piezo stack to be defined along with its geometry. For the following simulations, only material properties were changed, and the geometries were kept constant based on Table 2. The 'Simulation Parameters' input allows the driving frequency of the actuators, the return spring constant, the pre-tension, applied load, and the simulation time to be defined. The 'Piezo Response' section defines the time response properties as discussed in the previous section. The

'Iterative Solver' module takes all the inputs and performs six steps that define one inchworm period repeatedly until the simulation time duration is met. For each stage, the script tracks the location of the top brake and the time duration; these results are seen in Figure 14. Similar to the Step Size vs. Applied Force plot, only APC 856 and PZT-5H are competitive. This plot also helps show that even though APC 856 has a larger step size with heavier loads, it does not lead to a faster extension under minor load conditions. PZT-5H is able to move farter slightly in the one-second duration.

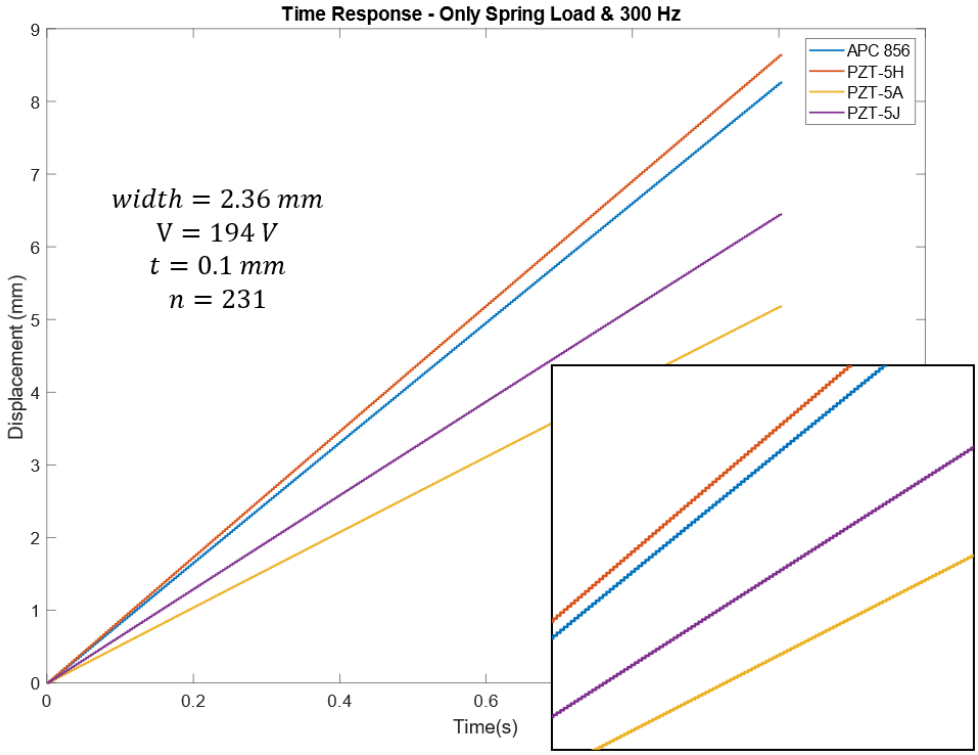

Figure 14: Time response of entire inchworm with only spring load.

Even though the lines appear to be smooth, they are composed of many small step changes. The vertical jumps correspond to the extender increasing in length, and the horizontal sections represent the time it takes for the brakes to engage and disengage. As the brakes are being actuated, the inchworm is stationary. Figure 14 shows how PZT-5H will allow for the design requirement of 8.80 mm/s extension speed to be reached when only a spring load is acting on the extender. To analyze how the performance will change once the full finger load of 10 N is applied, a second simulation is run comparing only the loaded and un-loaded PZT-5H configurations. As seen from Figure 15, the loaded inchworm only travels to roughly 5 mm in one second. This is quite a drastic reduction in performance but expected as it was loaded quite highly. The load of 10N would typically only be seen at the end of a grasping motion when the hand when the fingers have already made contact with an object. So, in reality, the actual operating curve should be closer to the 'Only

Spring Load' profile. This configuration of the extender piezo meets the design requirement of 8.80 mm/s of travel speed and still carrying 167 N.

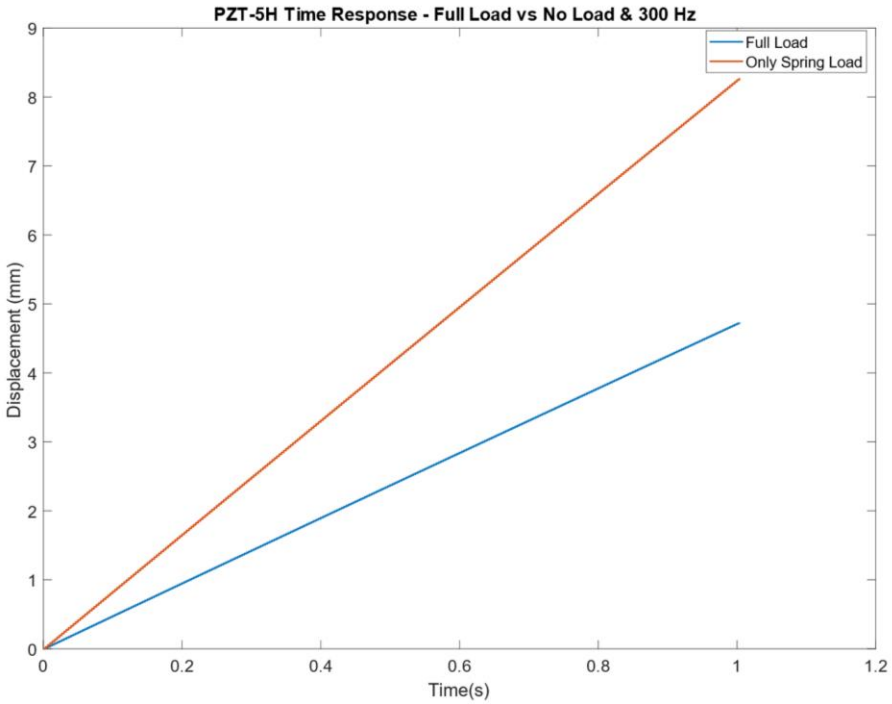

Figure 15: Time response of PZT-5H. Full load versus unloaded inchworm performance.

Having defined the geometries of the brake and extender in section 4 and validating their performance in section 5, the following section discusses the overall packing of the actuator.

6.0 Packaging & Prosthetic Overview

Figure 16 illustrates the overall dimensions of the inchworm actuator designed through this report.

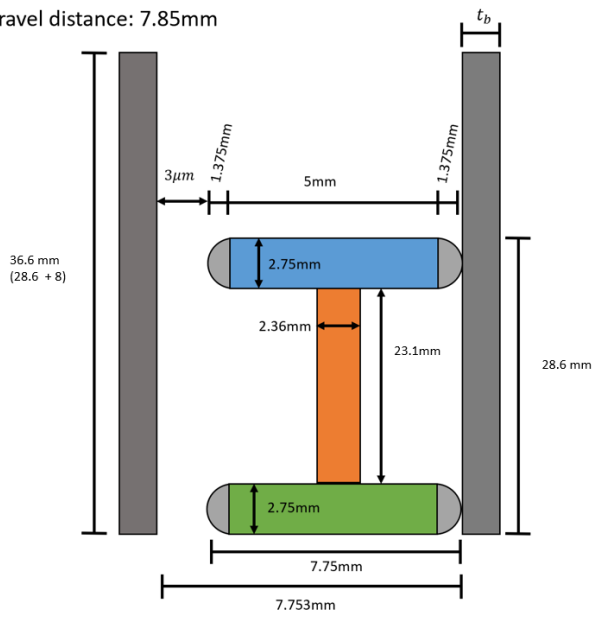

Figure 16: Overall inchworm dimensions.

The inchworm is relatively compact, at only 3 cm in length. It is designed to move through the tube with a diameter of 7.753 mm. This can be achieved by adding circular contact pads to the ends of the two brakes. Since the actuator only needs to move 7.35 mm to provide a 90-degree finger range of motion, the entire actuation system would be under 4 cm in length. A vital requirement of the success of prosthetic limbs is their mass requirement, and so to determine the mass of the inchworm system, the thickness of the travel tube needs to be determined. This was done by rough calculations shown in Figure 17.

Tube Thickness Approximation

- $F = 266\ N$
- $r = 2.75mm = 0.00275m$
- SAE 980X steel
  - $\sigma_y = 552\ MPa = 552 \times 10^6\ Pa$
- Case 1:
  - $\sigma_{max} = \frac{\frac{F}{2} \times r \times \left(\frac{t_b}{2}\right)}{\left(\frac{0.00275 \times t_b^3}{12}\right)}$
  - $t_b \geq \sqrt{\frac{3 \times F \times r}{0.00275 \times \sigma_y}} = 1.4275mm$
- Case 2:
  - $\sigma_{max} = \frac{F}{t_b(2 \times 0.00275)}$
  - $t_b \geq \frac{F}{\sigma_y(2 \times 0.00275)} = 0.0876mm$
- So, $t_b \geq 1.4275mm$ Therefore...
  - Let, $\boldsymbol{t_b = 3mm}$

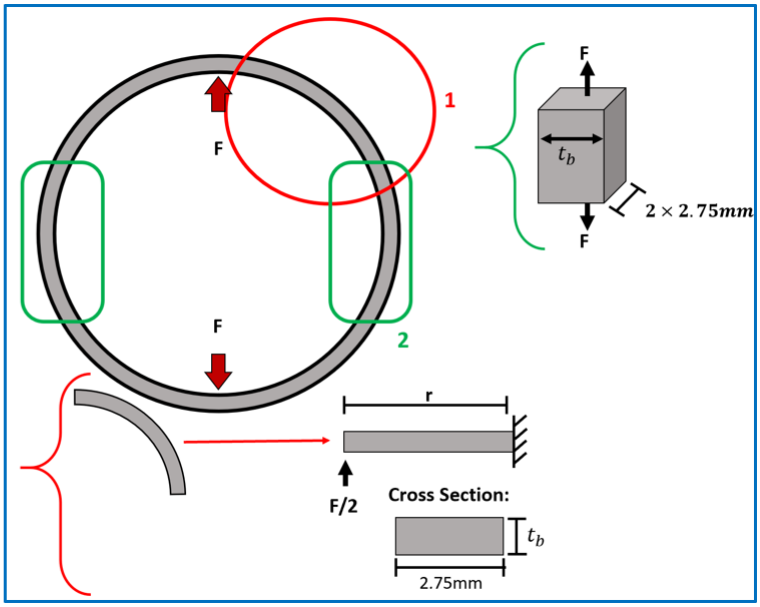

Figure 17: Inchworm actuator travel tube thickness.

As a worst-case scenario approximation, the side of the tube walls where the piezo brakes would be applying the force is assumed to be a simply supported beam; this results in a thickness requirement of 1.4 mm. To add a safety factor and ensure minimal deformation of the tube housing, its thickness is taken to be 3 mm. With this information, the overall system mass can be approximated given the geometries and densities of each material. The masses are shown in Table 4.

Table 4: Mass breakdown of inchworm actuator.

System-Level Mass Breakdown (grams)				
Brake Actuator	Extender Actuator	Contact Pads	Travel Tube	**Total Piezo Inchworm**
0.284	1.013	0.044	29.859	**31.614**

The heaviest component of the inchworm actuator system is the housing it travels along. This tube was assumed to be steel, but metals with lower densities would help reduce this mass. Scaling this concept up for all five fingers, the inchworm actuators would be able to articulate five 1-DOF fingers with a total mass of 158 grams.

7.0 Conclusion

This project looked to see if an inchworm actuator can be used to articulate a 1-DOF finger of a prosthetic hand. The first step in the process involved selecting design requirements based on a literature review. The two essential requirements were a finger closing speed of 100 deg/s and a grasping force of 10 N. Based on a model finger that is 80 mm long, an inchworm travel speed of 8.73 mm/s, and a carrying force of 167 N was derived. The front and rear inchworm brakes were designed to support the load of 167 N while allowing for a contraction of 3 μm. Excel calculators allowed for the material and geometry of the brakes to be determined. A similar approach was employed to design the extender piezo. A summary of the inchworm parameters is shown in Table 5.

Table 5: Summary of inchworm parameters.

	Brake Actuator	Extender Actuator
Driving Voltage	194	194
Material	APC 856	PZT-5H
Side Length (mm)	2.75	2.36
Thickness (mm)	0.1	0.1
Number of layers	50	231
Total Length (mm)	5	23.1
Extension Step Size (μm)	3.01	14.56

As seen from Figure 16, the overall inchworm is 3 cm tall and requires a 4 cm cylindrical tube to move within. The overall package is relatively light at only 31.2 grams and does not include any complicated mechanism that traditional prosthetic hands need. One major limitation of this design is that the finger is approximated as only 1-DOF. The next step would be trying to implement a second DOF and ensuring the structure still remains light. Another limitation is that the 3 μm clearance for the inchworm to travel through is a tight tolerance to keep. This design needs to be validated through testing to ensure the inchworm can move and does not seize up due to tolerancing issues.

8.0 References

Belter JT, Segil JL, Dollar AM, Weir RF. "Mechanical design and performance specifications of anthropomorphic prosthetic hands: a review." J Rehabil Res Dev. 2013;50(5):599-618. doi: 10.1682/jrrd.2011.10.0188. PMID: 24013909.

Braza, Diane W., and Jennifer N. Yacub Martin. "Upper Limb Amputations". Essentials Of Physical Medicine And Rehabilitation, 2020, pp. 651-657. Elsevier, doi:10.1016/b978-0-323-54947-9.00119-x. Accessed 24 Jan. 2021.

Edinger B., Frecker M., and Gardner J., "Dynamic Modeling of an Innovative Piezoelectric Actuator for Minimally Invasive Surgery," *Journal of Intelligent Materials Systems and Structures*, vol. 11, no. 10, pp. 765–770, Oct. 2000, doi: 10.1177/104538900772663801.

"Friction and Friction Coefficients." Engineeringtoolbox.com, 2021, www.engineeringtoolbox.com/friction-coefficients-d_778.html. Accessed 26 Apr. 2021.

Levinson, Jacob. "Design and Control of a Robotic Thumb Using Piezoelectric Actuators." https://dspace.mit.edu/bitstream/handle/1721.1/54514/558954240-MIT.pdf?sequence=2&isAllowed=y. Accessed 24 Jan. 2021

Ling S.F., Du H., and Jiang T., "Analytical and experimental study on a piezoelectric linear motor," *Smart Materials and Structures*, vol. 7, no. 3, pp. 382–388, Jun. 1998, doi: 10.1088/0964-1726/7/3/012.

Mishra, Suvrajyoti et al. "Advances In Piezoelectric Polymer Composites For Energy Harvesting Applications: A Systematic Review". *Macromolecular Materials And Engineering*, vol 304, no. 1, 2018, p. 1800463. *Wiley*, doi:10.1002/mame.201800463.

PI Ceramic. "Dynamic operation." https://www.piceramic.com/en/piezo-technology/properties-piezo-actuators/dynamic-operation/. Accessed 7 Apr. 2021.

PI USA. "P-882 – P-888 PICMA® Stack Multilayer Piezo Actuators." https://www.pi-usa.us/en/products/piezo-actuators-stacks-benders-tubes/p-882-p-888-picma-stack-multilayer-piezo-actuators-100810/#description. Accessed 7 Apr. 2021